

A Numerical Study of the Track Deflection of Supertyphoon Haitang (2005) Prior to Its Landfall in Taiwan

GUO-JI JIAN

Central Weather Bureau, Taipei, Taiwan

CHUN-CHIEH WU

Department of Atmospheric Sciences, National Taiwan University, Taipei, Taiwan

(Manuscript received 3 January 2007, in final form 4 June 2007)

ABSTRACT

A series of numerical simulations are conducted using the advanced research version of the Weather Research and Forecasting model with a 4-km fine mesh to examine the physical processes responsible for the significant track deflection and looping motion before the landfall of Supertyphoon Haitang (2005) in Taiwan, which poses a unique scientific and forecasting issue. In the control experiment, a low-level northerly jet induced by the channeling effect forms in the western quadrant of the approaching storm, where the inner-core circulation is constrained by the presence of Taiwan's terrain. Because of the channeling effect, the strongest winds of the storm are shifted to the western portion of the eyewall. The northerly advection flow (averaged asymmetric winds within 100-km radius) results in a sharp southward turn of the westward-moving storm. The time series of the advection flow shows that the advection wind vectors rotate cyclonically in time and well match the motion of the simulated vortex during the looping process. A sensitivity study of lowering the Taiwan terrain elevations to 70% or 40% of those in the control experiment reduces the southward track deflection and loop amplitude. The experiment with the reduced elevation to 10% of the control experiment does not show a looping track and thus demonstrates the key role of the terrain-induced channeling effect. Experiments applying different values of the structure parameter α illustrate that increasing the strength, size, and translation speed of the initial storm results in a smaller interaction with Taiwan's terrain and a smaller average steering flow caused by the asymmetric circulation, which leads to a proportionally smaller southward track deflection without making a loop.

1. Introduction

Landfalling tropical cyclones (TCs) often produce immense damage through their strong winds, torrential rains, and storm surges. Recently, the research of TC landfall has received much attention, especially as one of the primary foci in the U.S. Weather Research Program (USWRP; Marks and Shay 1998; Elsberry and Marks 1999). During the landfall period, the TC inner core often has a highly asymmetric distribution of strong winds and deep convection. When the TC approaches a region with complex terrain, the asymmetric structures may become more complicated and result in various types of track deflections. A detailed

investigation of such track deflections is of great importance to hazard mitigation because the most severe damage appears to be highly related to the landfall location and the landfall time.

During 1958–2005, Taiwan was struck by 161 typhoons, with 86 of them making landfall (TC center crossed land) on the island. Thus, Taiwan is a region suffering from a very high frequency of TC strikes. In addition, Taiwan has a complex terrain (Fig. 1b). Approximately 70% of the total land area consists of mountains, with the highest peak of 3952 m above sea level at Yushan. The impact of the Central Mountain Range (CMR) of Taiwan on typhoons is an interesting research topic (Wu and Kuo 1999), in part because of the complex interactions between the storm and the topographic barrier. Mesoscale phenomena are believed to cause deflections and discontinuities of the TC track (e.g., Brand and Brelloch 1974; Wang 1980), the

Corresponding author address: Dr. Guo-Ji Jian, Central Weather Bureau, No. 64, Gongyuan Road, Taipei, Taiwan.
E-mail: jgj@cwb.gov.tw

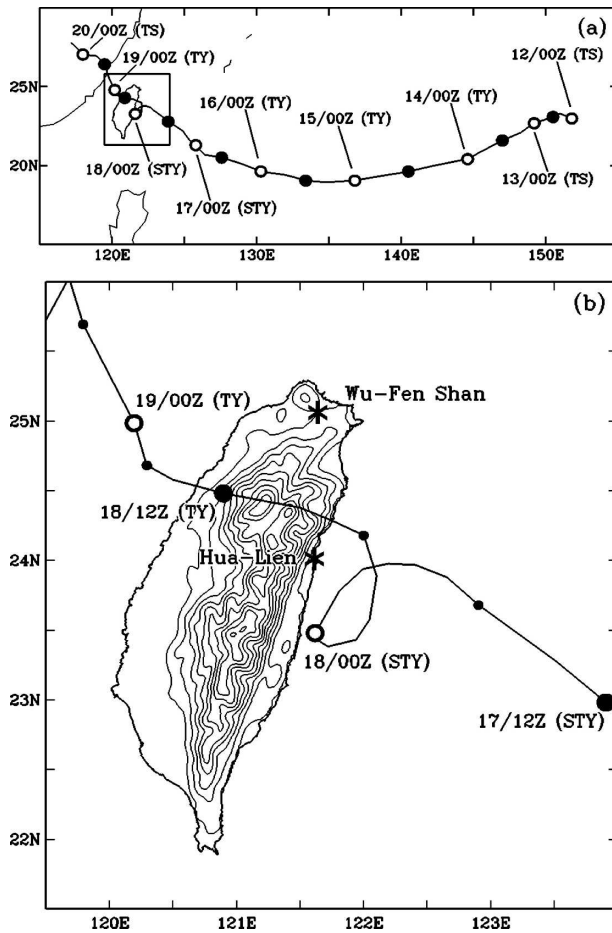


FIG. 1. (a) Best track of Supertyphoon Haitang (2005) from 0000 UTC 12 Jul to 0600 UTC 20 Jul. Open circles are the 0000 UTC center positions, and large solid circles are the 1200 UTC positions. (b) Supertyphoon Haitang made a slow cyclonic loop off the eastern coast of Taiwan. Small solid circles are the best-track positions at 0600 and 1800 UTC. The two asterisk symbols are the locations of Wu-Fen-Shan and Hua-Lien Doppler radar stations. The Taiwan terrain heights (thin lines) start from 200 m high and have a contour interval of 300 m.

formation of mesoscale leeside vortices (e.g., Wang 1980), and the phase-locked distribution of torrential rains (e.g., Chang et al. 1993; Wu and Kuo 1999).

Both observational (e.g., Brand and Brelloch 1974; Wang 1980) and modeling approaches (e.g., Chang 1982; Bender et al. 1987; Yeh and Elsberry 1993a,b; Lin et al. 1999; Wu 2001; Wu et al. 2002; Peng and Chang 2002; Jian et al. 2006) have been employed to examine the influence of the CMR on TC track deflection and continuity, and extensive reviews of these approaches and results are provided by Wu and Kuo (1999) and Lin et al. (2005). A large number of the past studies have revealed that the weaker and slower-moving TC is more susceptible to the topographic deflection. By con-

trast, more intense and rapidly moving TCs are more likely to move across the CMR with a continuous track. Yeh and Elsberry (1993a,b) suggested that a westward-moving storm tends to be decelerated and deflected southward upstream of Taiwan when the basic flow and outer cyclone circulation are blocked and perturbed by the CMR. The storm will subsequently be deflected northward as it approaches the southern or central parts of Taiwan via an advection flow associated with an asymmetric flow created by an imbalance in the inner-core region.

Lin et al. (1999) found that the orographic blocking and channeling effects lead to a southward deflection of the small vortex regardless of its initial strength and translation speed. Applying the Buckingham- Π theorem, Lin et al. (2005) identified six nondimensional control parameters for diagnosing track deflections and continuity of a westward-moving vortex across the CMR. They indicated that the vortex would experience a larger (smaller) deflection, and the vortex track becomes discontinuous (continuous), with a combination of smaller (larger) values of V_{\max}/Nh , U/Nh , R_{\max}/L_y , U/fL_x , and V_{\max}/fR_{\max} , and a larger (smaller) value of h/L_x , where V_{\max} is the maximum tangential wind and R_{\max} is the radius of V_{\max} ; N is the Brunt-Väisälä frequency; h is the mountain height; U is the basic flow speed; f is the Coriolis parameter; and L_x and L_y are the horizontal scales of the mountain in the x and y directions, respectively. Physically, V_{\max}/Nh and V_{\max}/fR_{\max} represent the vortex Froude number and nondimensional vorticity of the inner core of the TC, and U/Nh and U/fL_x are the Froude number and Rossby number associated with the basic flow. The h/L_x and R_{\max}/L_y are the measures of topographic steepness and the ratio of the TC scale to mountain scale.

The 2005 typhoon season was exceptional because three named supertyphoons (Haitang, Talim, and Longwang) made landfall in Taiwan with serious consequences. This study particularly focuses on the cyclonic looping motion of Supertyphoon Haitang prior to its landfall in Taiwan (Fig. 1), which poses a rather unique scientific and forecasting problem. Although Haitang moved in a general northwestward direction from 17 to 20 July 2005 (see Fig. 1a), Doppler radar observations indicated that Haitang made a counterclockwise loop for about 8–9 h as the center was approximately 50 km east of Hua-Lien (Figs. 1b and 2). A similar cyclonic loop before landfall in Taiwan has been found in some other supertyphoons [e.g., Shirley (1960), Mary (1965), and Sarah (1989)]. Such supertyphoons pose severe threats to Taiwan because of the long duration heavy rainfall, sustained strong winds, devastating flash flooding, and landslides. As a result, it

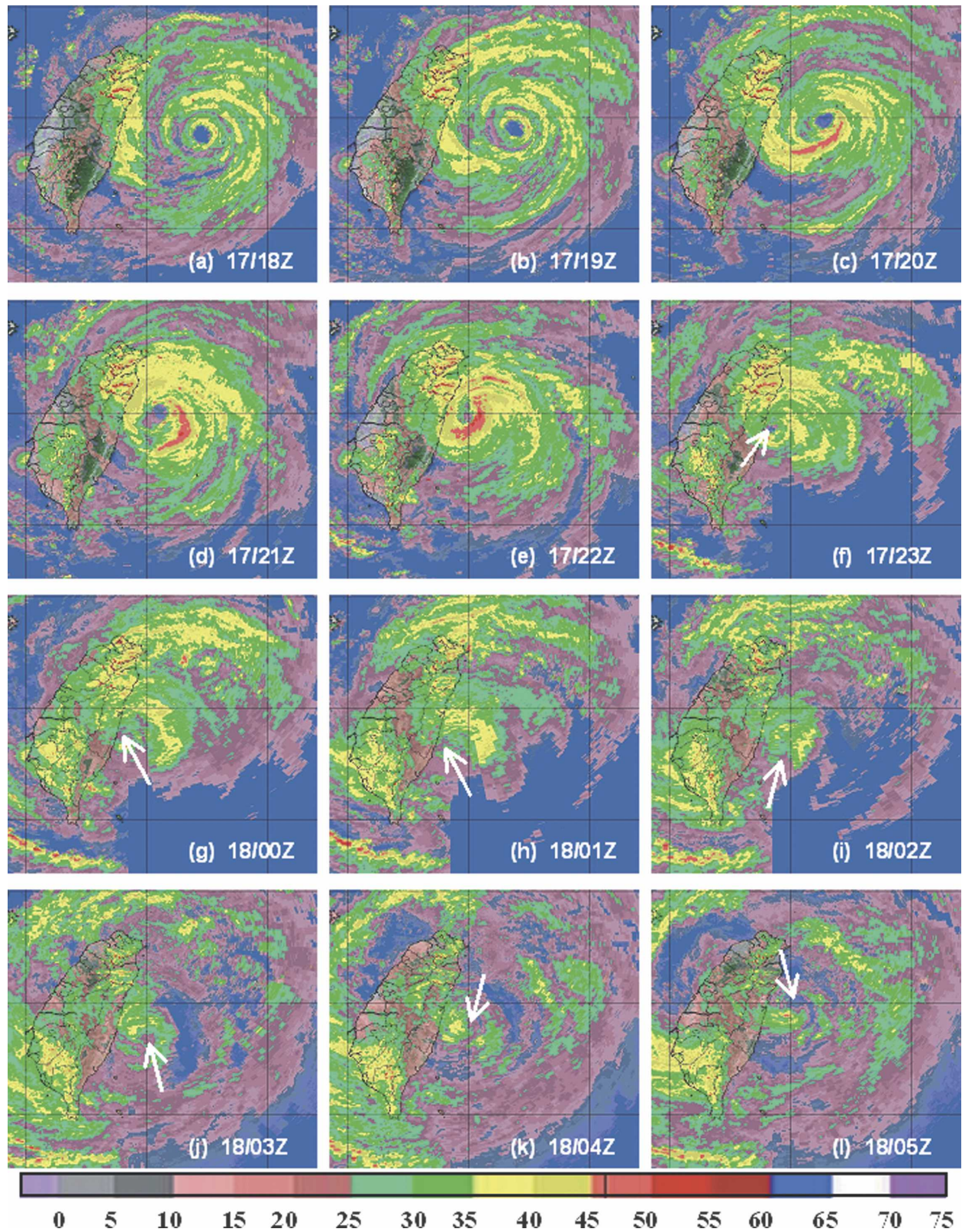


FIG. 2. Composite of vertical maximum values of radar reflectivity (dBZ) near the Taiwan area. The times of observations are shown in UTC in the lower-right corner of each image. The arrows in the last seven images indicate the center of Haitang.

is important to understand the dynamics involved in the looping motion during the approach of a TC.

In the present study, a series of high-horizontal-resolution (4 km) simulations of Haitang are made using the newly developed advanced research version of the Weather Research and Forecasting (WRF-ARW) model (Skamarock et al. 2005). The following questions are addressed: 1) What dynamical processes are responsible for Haitang's track deflection before landfall in Taiwan? 2) What is the role played by Taiwan's terrain? 3) What is the impact of the vortex structure, that is, with different values of structure parameter in the initial vortex?

This paper is organized as follows. Section 2 gives a brief overview of Haitang. Section 3 describes the model setup and experiment design. The numerical results are discussed in section 4. Discussion and conclusions are provided in section 5.

2. Overview of Supertyphoon Haitang

Haitang developed from a tropical disturbance at the subtropical latitude (23°N) and was upgraded to a tropical storm¹ (17 m s^{-1}) at 0000 UTC 12 July. A subtropical high centered south of Japan led to a primary steering current that guided Haitang on a slightly curving track across the western North Pacific (Fig. 1a). Haitang was upgraded to typhoon strength (33 m s^{-1}) at 1800 UTC 13 July while located approximately 900 km north-northeast of Guam. After turning westward and continuing to strengthen, Haitang became a super-typhoon (51 m s^{-1}) at 0600 UTC 16 July. Haitang reached peak intensity at 1500 UTC 16 July with an estimated maximum sustained wind of 55 m s^{-1} (10-min-averaged wind) and a minimum mean sea level pressure (MSLP) of 912 hPa. On 17 July, it veered to a north-westward track and approached the east coast of Taiwan.

As Haitang approached Taiwan, continuous radar coverage of the eyewall and the inner rainbands was provided by the radars at Wu-Fen-Shan [Weather Surveillance Radar-1988 Doppler (WSR-88D)] and Hua-Lien [Germany's meteorological Doppler radar (METEOR 1000S); see Fig. 1b for locations]. The Doppler observations document the sharp southward turn and slow cyclonic loop off the eastern coast of Taiwan between 2300 UTC 17 July and 0700 UTC 18 July (Figs. 1b and 2). The eyewall had a radius of approximately 40–50 km at around 2200 UTC 17 July. The center made landfall about 30 km north of Hua-

Lien at around 0650 UTC 18 July and caused 12 deaths as well as estimated property damage of at least \$150 million (U.S. dollars) in the Taiwan area. Thereafter, Haitang was downgraded to a typhoon while moving across the CMR, and further weakened to a tropical storm at 0600 UTC 19 July. Finally, Haitang made a second landfall over the Fujian province of China and then became a tropical depression at 1200 UTC 20 July.

3. Model description and experiment design

a. Model configuration and initial conditions

The numerical simulations presented in this study have been conducted with the WRF-ARW modeling system, version 2.0.3 (Skamarock et al. 2005). The WRF-ARW system solves the compressible, nonhydrostatic, flux-form Euler equations in a terrain-following, hydrostatic-pressure vertical coordinate (η coordinate). The model domains (Fig. 3a) are a stationary 4-km mesh (121×121) nested within a 12-km (191×191) mesh using a two-way interactive method. Both domains extend vertically to 100 hPa and are resolved by 31 η levels, with 8 levels in the lowest 1 km. The model topography (see Fig. 1b for Taiwan's terrain in the inner domain with 4-km resolution) is interpolated from terrain data with 30'' resolution. Information on land use is obtained from the U.S. Geological Survey (USGS) with the same resolution as for the topography.

The physics of the model include the WRF single-moment five-class microphysics (Hong et al. 2004), Yosei University planetary boundary layer (PBL) scheme (Hong et al. 2003), five-layer soil model (Chen and Dudhia 2000), Rapid Radiative Transfer Model longwave radiation (Mlawer et al. 1997), and Dudhia shortwave radiation scheme (Dudhia 1989). The modified version of Kain–Fritsch convective parameterization (Kain 2004) is also used in outer domain. The model initial conditions are taken from the operational Central Weather Bureau (CWB) Nonhydrostatic Forecasting System (NFS) analyses, which are available every 12 h on a $15\text{ km} \times 15\text{ km}$ grid. A typhoon bogusing scheme [National Center for Atmospheric Research–Air Force Weather Agency (NCAR–AFWA) scheme; Davis and Low-Nam 2001] is employed in this study to enhance the description of the initial model vortex. The lateral boundary conditions are obtained from the operational NFS forecast at 6-h intervals.

b. Design of numerical experiments

A series of 72-h integration experiments (Table 1) are initialized at 0000 UTC 17 July 2005 when Haitang was at its most developed stage, which is favorable for implanting the synthetic vortex into the model. In ad-

¹ Tropical storm: wind speed of $17\text{--}32\text{ m s}^{-1}$; typhoon: wind speed of $33\text{--}50\text{ m s}^{-1}$; supertyphoon: wind speed of 51 m s^{-1} or higher.

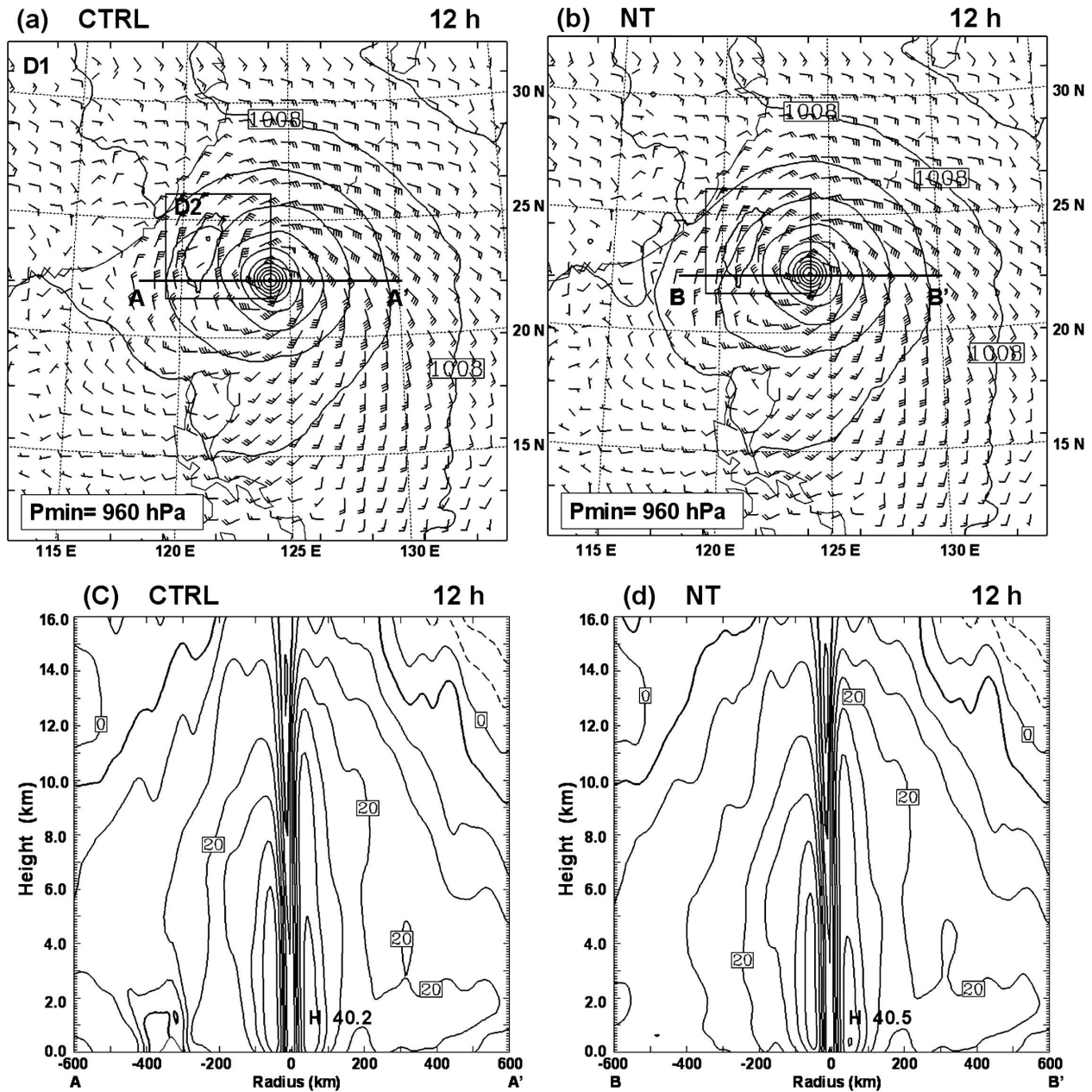


FIG. 3. Simulated wind vectors (one full wind barb = 5 m s^{-1}) at the lowest model level and sea level pressure (contour interval of 4 hPa) from experiments (a) CTRL and (b) NT after a 12-h model simulation. Domain configuration for WRF-ARW simulations is also shown in (a). Vertical cross sections of tangential winds (contour interval of 5 m s^{-1}) along AA' and BB' from experiments (c) CTRL and (d) NT.

dition, the main interest of this study is the looping motion before Haitang's landfall in Taiwan, which took place at 2300 UTC 17 July. The initial time chosen appears appropriate for studying the dynamics involved in the significant track deflection. Details of all the experiments are described as below (see Table 1).

- CTRL: this control experiment includes the full Taiwan terrain and applies the NCAR-AFWA bogusing

scheme (Davis and Low-Nam 2001) to implant an initial Rankine vortex into the operational CWB NFS analysis. The Rankine vortex is

$$V(r) = V_{\max} \left(\frac{r}{R_{\max}} \right), \quad 0 < r \leq R_{\max}, \quad (1)$$

$$V(r) = V_{\max} \left(\frac{R_{\max}}{r} \right)^{\alpha}, \quad R_{\max} \leq r, \quad (2)$$

TABLE 1. Description of numerical experiments.

Expt	Topography in Taiwan	Bogused vortex
CTRL	Full topography	Control vortex structure ($\alpha = 0.60$)
H70	70% of the CTRL	As in CTRL
H40	40% of the CTRL	As in CTRL
H10	10% of the CTRL	As in CTRL
FLAT	1-m terrain	As in CTRL
NT	No terrain (ocean)	As in CTRL
A35	As in CTRL	$\alpha = 0.35$
A47	As in CTRL	$\alpha = 0.47$
A35_NT	No terrain (ocean)	As in A35
A47_NT	No terrain (ocean)	As in A47

where V_{\max} is the maximum tangential wind speed, R_{\max} is the radius of maximum wind (RMW). The shape parameter α in (2) varies typically between 0.5 and 0.7 (Miller 1967). In CTRL, V_{\max} , R_{\max} , and α for a typical supertyphoon are specified as 53 m s^{-1} , 50 km, and 0.6, respectively.

- H70, H40, and H10: these experiments are the same as in CTRL, except the terrain height of Taiwan at each grid point is reduced to 70%, 40%, and 10% of the value in CTRL, respectively.
- FLAT: this experiment is the same as in CTRL, except that the Taiwan terrain is set to 1-m elevation, while the land–sea attributes remain unchanged.
- NT: this experiment is the same as in CTRL, except that the Taiwan terrain is switched to the ocean conditions.
- A35 and A47: these experiments are the same as in CTRL, except that the value of α in the bogused vortex is set to 0.35 and 0.47, respectively.
- A35_NT and A47_NT: these experiments are the same as in NT, except that the value of α in the bogused vortex is set to 0.35 and 0.47, respectively.

Comparisons of the above numerical experiments are expected to improve understanding of the factors affecting Haitang's track near Taiwan, such as the role of the terrain height of Taiwan, and the impact of the vortex structure, that is, with different values of α in the initial vortex.

4. Results

a. Experiments CTRL and NT

After a 12-h integration for the model to adjust the mass and wind fields, the MSLP and wind fields are well simulated by the CTRL (Figs. 3a,c) and NT experiments (Figs. 3b,d), except for the region near Taiwan where the outer storm circulation of CTRL is markedly perturbed by the CMR. Before making landfall in Tai-

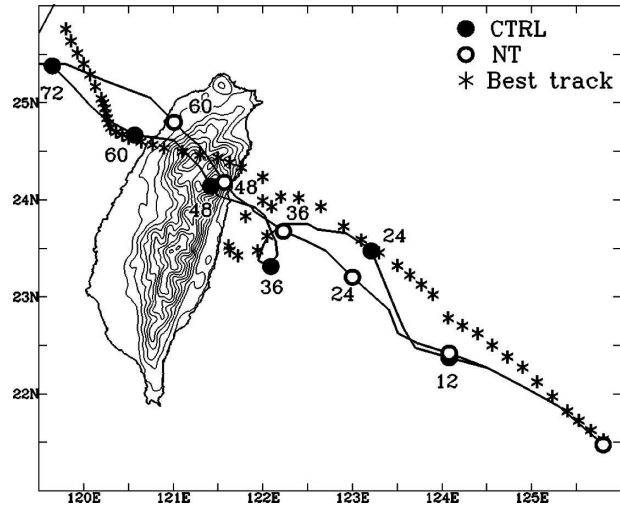


FIG. 4. Simulated tracks in the CTRL (solid circles) and NT (open circles) experiments. The asterisk symbols are the best-track positions every 1 h from 0000 UTC 17 Jul to 0600 UTC 19 Jul. The Taiwan terrain heights (thin lines) in experiment CTRL start from 200 m high and have a contour interval of 300 m. Both of the 72-h model simulations begin at 0000 UTC 17 Jul 2005.

wan, the simulated typhoon center is defined if both the minimum MSLP center and circulation center at the lowest model level exist and are collocated. Because these centers are not collocated while the typhoon is moving across the CMR, the typhoon center is then defined as the circulation center based on the streamline analysis.

The storm track in CTRL (Fig. 4) generally mimics the best-track positions (Fig. 1b) throughout the 72-h simulation. The cyclonic looping path and the landfall location agree well with the observed best track. Because the model storm motion in CTRL is slower than the best track during the first 18 h of the integration (the model spinup period), the landfall in Taiwan is about 10 h later than observed. Despite this slow bias, the simulation results still provide useful information in evaluating the physical processes causing Haitang's track deflection when the simulated storm approaches the east coast of Taiwan. In the absence of the Taiwan terrain (NT), the simulated storm moves toward the northwest following a straight track (Fig. 4). Haitang's looping motion is not predicted in the NT simulation.

It is noteworthy that a more northward track is simulated before the looping motion in the CTRL (from 15 to 24 h; see Fig. 4) compared with the northwestward track for the storm in the NT experiment. One may infer that the initialization of the flow with the Taiwan terrain may introduce an imbalance and lead to a long-term oscillation in the simulated track (i.e., northward during the first 18 h and then southward in the next 18

h). To examine this possible factor, two additional experiments are performed by starting the integration 24 h earlier than the CTRL and NT simulations. A more northward track and a cyclonic looping path still exist in the modified CTRL when the simulated storm moves closer to the Taiwan terrain (not shown). This suggests that the more northward track deflection before the loop in the CTRL is mainly caused by a northward circulation to the east of Taiwan that results from the interaction between the flow and the Taiwan terrain (e.g., Chang 1982; Bender et al. 1987).

The simulated reflectivity (composite of vertical maximum values), wind vectors (at the lowest model level), and MSLP distributions in experiment CTRL are shown in Fig. 5 every 3 h from 27 to 42 h. Between 27 and 33 h, the CTRL simulation has realistic terrain-enhanced rainbands over northeastern Taiwan as compared with the observed radar reflectivity from 1800 to 2300 UTC 17 July (Fig. 2). When the terrain of Taiwan is removed, the eyewall convection and the convective bands over windward mountain slopes are weaker (not shown). At 30 h, the simulated storm center in CTRL (Fig. 5b) is at about 70 km east of Hua-Lien, with stronger spiral bands along the northeastern and southeastern quadrants of the eyewall. These inner rainbands are quite similar to those observed by Doppler radar at 2200 UTC (Fig. 2). During the next few hours, both the CTRL (Figs. 5c–f) and the actual storm (after 2200 UTC; Fig. 2) are suddenly deflected southward and make a cyclonic loop before finally making landfall in Taiwan. Since the CTRL is able to reasonably simulate Haitang's movement, the CTRL simulation is studied to understand the physical mechanisms responsible for the impact of the presence of Taiwan's terrain on the looping motion of Haitang.

The west–east vertical cross section of tangential wind speed through the storm center for the CTRL is displayed at 1-h intervals in Fig. 6. Before 30 h, the region of stronger winds is on the eastern side of vortex center. During 31 to 33 h, the region of stronger winds in the CTRL simulation shifts to the western side of the vortex center (Figs. 6d–f) just as the storm is beginning to be deflected southward (see Fig. 4). The low-level winds on the western side of the eyewall are strongly enhanced between the CMR and the storm, which results in a low-level northerly jet as shown in Fig. 6. This simulation is in agreement with Lin et al. (1999), who showed that the formation of the northerly jet is related to the orographic blocking and channeling effects. No northerly jet is present when the Taiwan terrain is excluded in the NT simulation (not shown).

The low-level jet is hypothesized to have an important role in the Haitang track deflection as it ap-

proaches Taiwan. Simple mass conservation principles imply that the along-streamflow is inversely proportion to the size of the cross section between the storm and the terrain. Lagrangian trajectory diagnostics of the hourly WRF-ARW output is used as the input to the read/interpolate/plot (RIP; see <http://www.mmm.ucar.edu/wrf/users/docs/ripug.htm>) utility to perform the backward trajectory calculation. The 3-h backward trajectories (starting at 33-h simulation time) for air parcels between 900- and 850-hPa pressure levels reach the western side of the storm in CTRL (Fig. 7) while experiencing substantial confluence. These parcels also undergo gradual ascent associated with the storm outer circulation, as the backward trajectories ending at 32 h (marked by small solid dots in Fig. 7) show that the parcels originally released from 900- and 850-hPa pressure levels can be traced back to be between 965 (Fig. 7a) and 950 hPa (Fig. 7b), respectively. Whereas the mean wind speed of the parcels at 32 h is around 35 m s^{-1} , the parcels at 33 h have speeds near 55 m s^{-1} .

These backward trajectories support the hypothesis that the channeling effect has a dominant role in the formation of the low-level northerly jet on the western side of the eyewall when these low-level air parcels accelerate from a wider to a narrower cross section. In the experiment without the Taiwan terrain (not shown), the trajectories are almost parallel. Consequently, the interaction of Taiwan's terrain with the typhoon circulation is critical to the formation of the low-level northerly jet. It is noteworthy that the above comparison of CTRL and NT cannot immediately distinguish which of the following two factors is the dominant effect: the removal of the Taiwan terrain or the change of the land attributes of the island to ocean. To address this issue, a detailed comparison of CTRL with FLAT is discussed in section 4b.

It is generally considered that to first-order the tropical cyclone motion is governed by the environmental steering or advection flow, which Chan and Gray (1982) defined as the tropospheric-average wind in a ring with a radius of 5° – 7° latitude. Neumann (1979) showed that the steering concept can account for about 80% of the variability in the 24-h tropical cyclone motion. Previous studies (e.g., Chan and Williams 1987; Fiorino and Elsberry 1989; Willoughby 1990, 1992; Yeh and Elsberry 1993b; Wu and Wang 2001a,b) have described mechanisms responsible for the change of the steering (advection) flow. For example, Chan and Williams (1987) and Fiorino and Elsberry (1989) showed that a pair of asymmetric gyres (beta gyres) causes the northwestward movement of the TC in a zero background flow on a beta plane. Several other physical processes, such as the interaction of the background

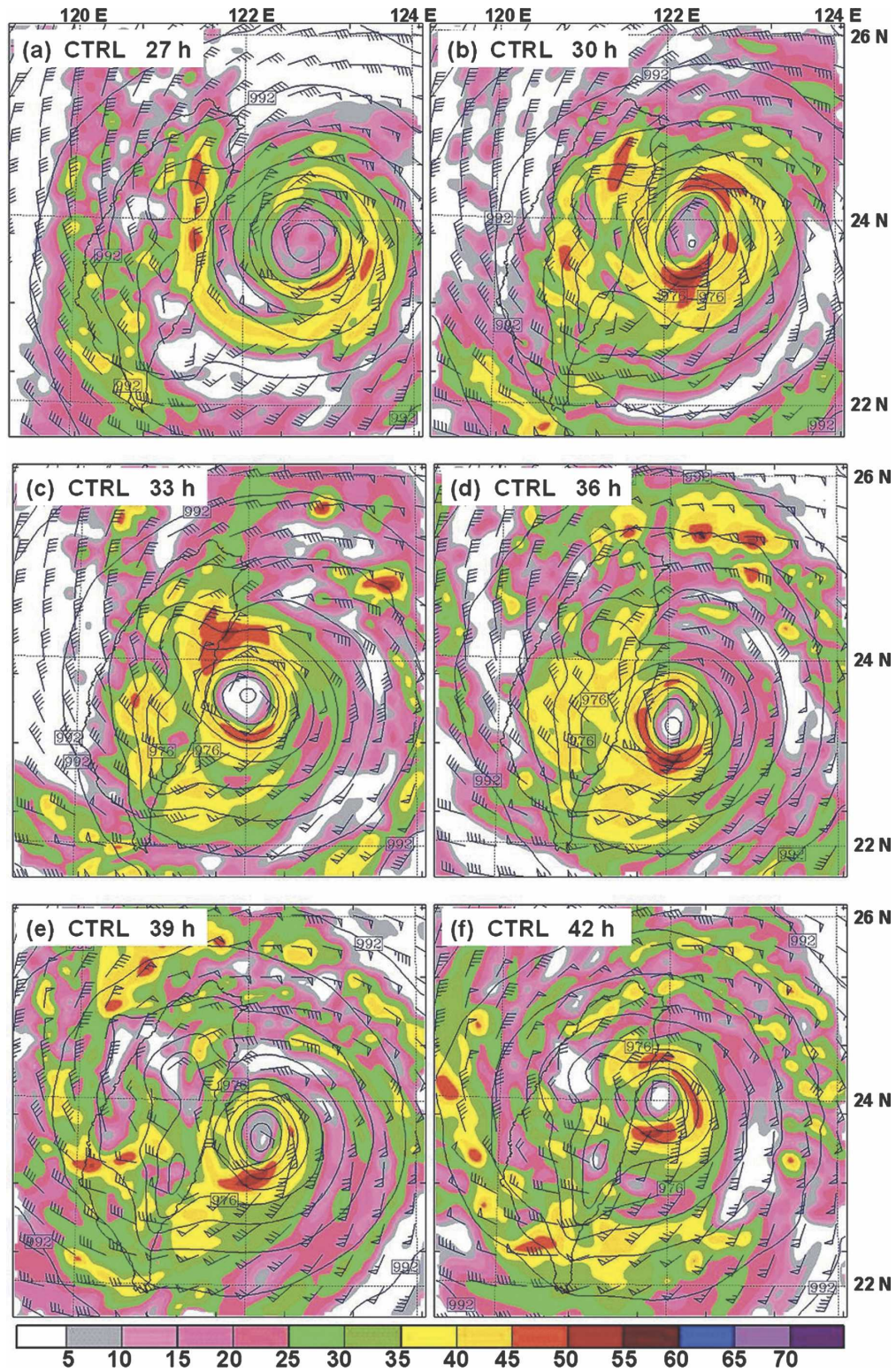


FIG. 5. Simulated radar reflectivity (composite of vertical maximum values; dBZ), wind vectors (one full wind barb = 5 m s^{-1}) at the lowest model level, and sea level pressure (contour interval of 4 hPa) from the CTRL at (a) 27, (b) 30, (c) 33, (d) 36, (e) 39, and (f) 42 h.

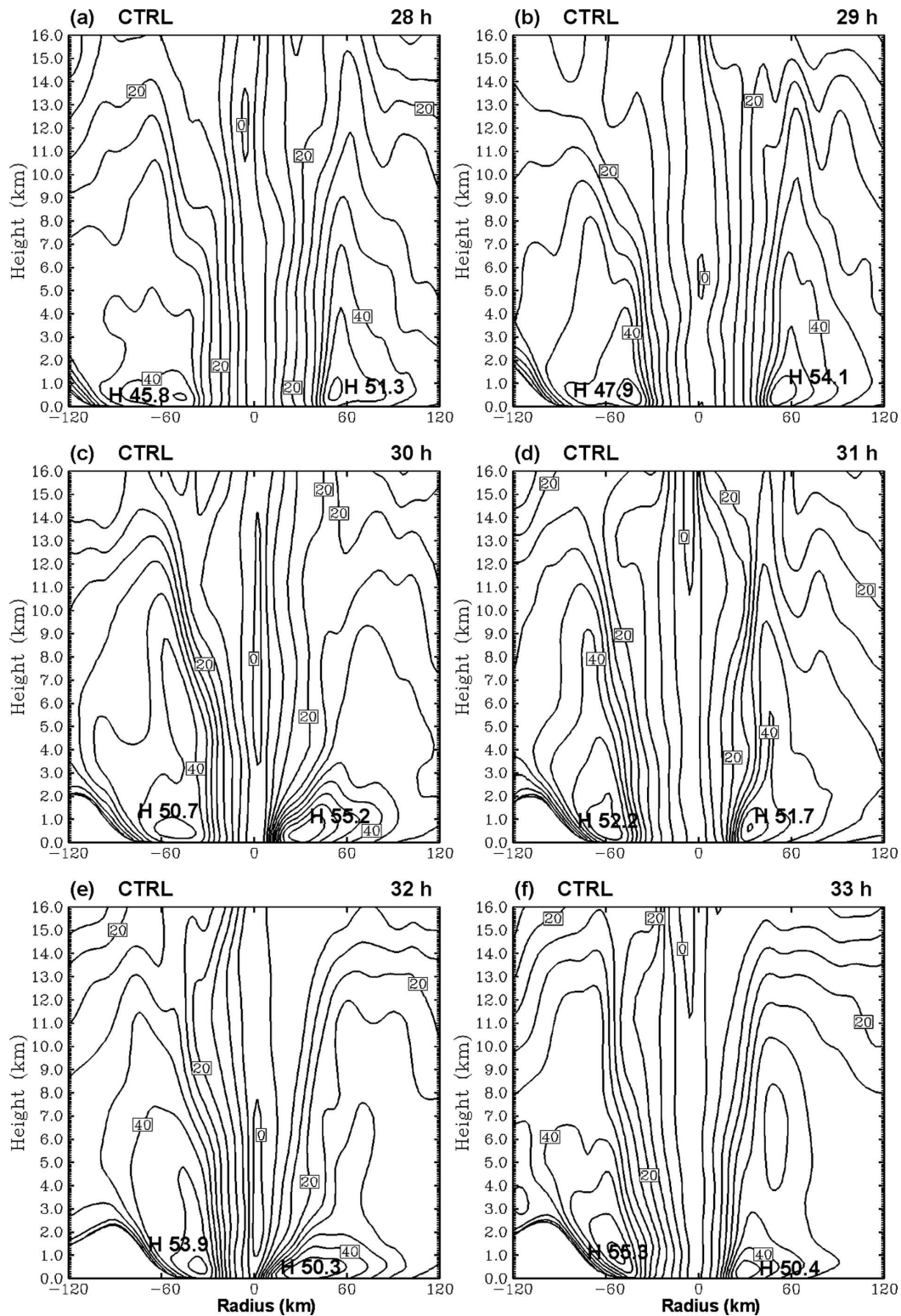


FIG. 6. West-east vertical cross sections of tangential wind speed (with contour interval of 5 m s^{-1}) cutting through the storm center in the CTRL at (a) 28, (b) 29, (c) 30, (d) 31, (e) 32, and (f) 33 h.

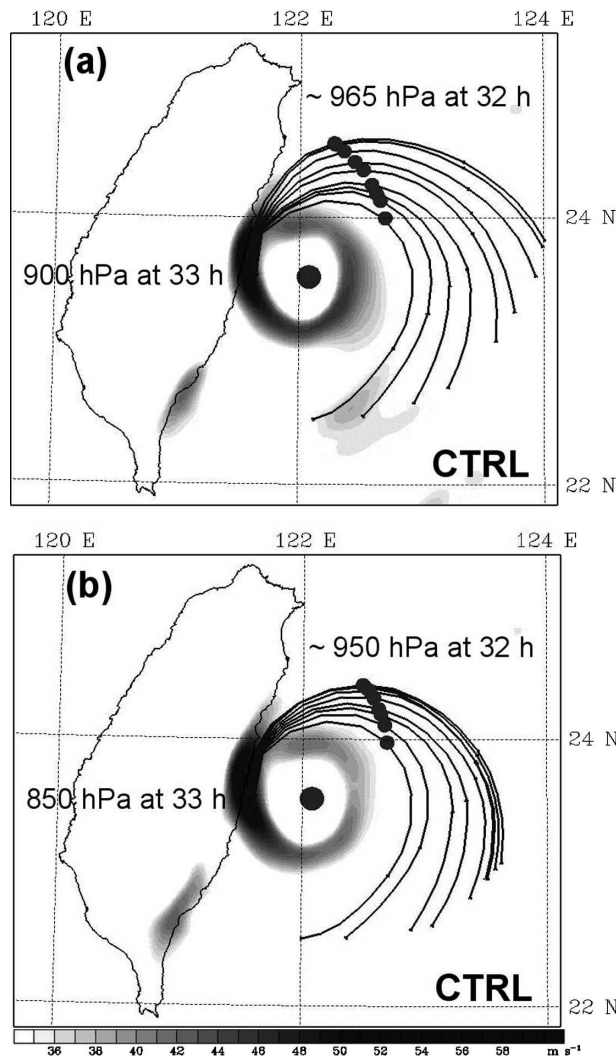


FIG. 7. Backward trajectories based on the WRF-ARW simulated winds from experiment CTRL. Parcels (small solid circles) are released at (a) 900- and (b) 850-hPa pressure levels at 33 h and calculated backward for 3 h. Horizontal wind speeds are shaded for values greater than 36 m s^{-1} (as shown in the grayscale). The large solid circle is the location of storm center at 33 h.

vertical wind shear with the baroclinic hurricane vortex (Wu and Emanuel 1993), asymmetric convection in the eyewall (e.g., Wu and Wang 2001a), the vertical tilt of a TC (e.g., Wu and Wang 2001b), and the imbalance in the inner structure of a TC approaching the mountain range (e.g., Yeh and Elsberry 1993b), may also play important roles in changing the advection flow.

In this study, another possible mechanism that results in an asymmetric (advection) flow is examined. The simulated winds at 700 hPa in the CTRL (Fig. 8a) are quite asymmetric with a local wind maximum of around 51 m s^{-1} to the west-northwest. Because the storm in CTRL is centered approximately 50–60 km east of Tai-

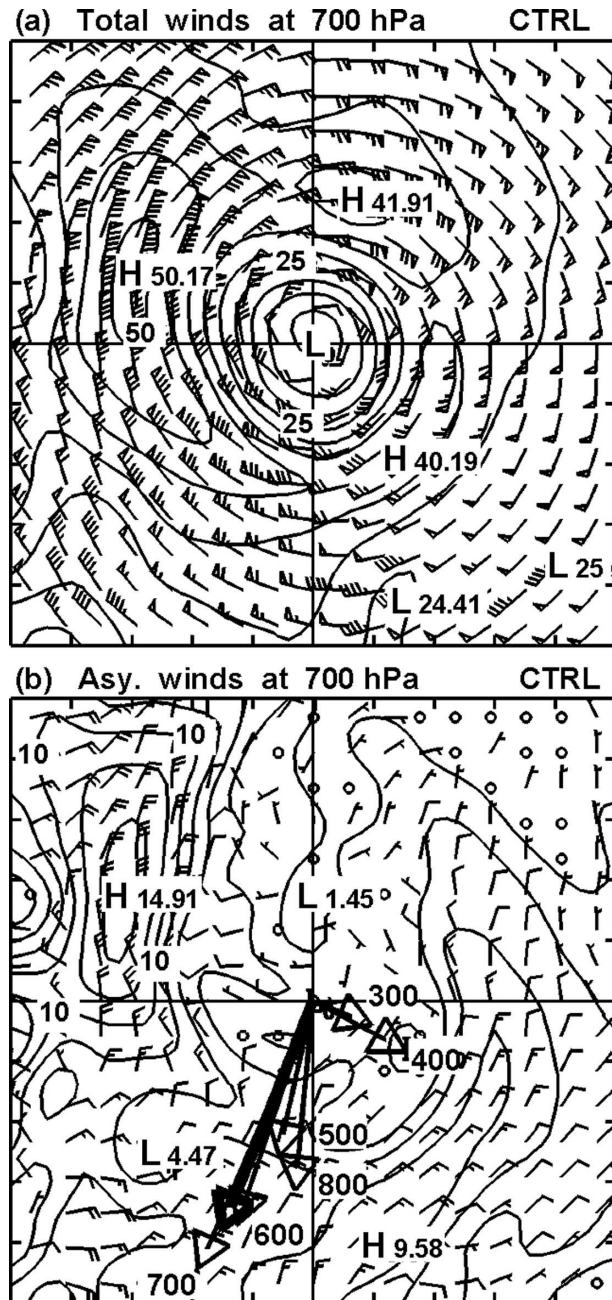


FIG. 8. (a) Simulated total wind fields (contour interval of 5 m s^{-1}) and (b) the asymmetric wind fields (contour interval of 2 m s^{-1}) at 700 hPa from experiment CTRL after 33-h model simulation (one full wind barb = 5 m s^{-1}). The boldface arrow in (b) indicates the storm motion vector (3.3 m s^{-1}). The open arrows show the average asymmetric flow within 100-km radius from the storm center at the indicated vertical levels (hPa). The domain in each panel is $200 \text{ km} \times 200 \text{ km}$.

wan at 33 h, the strong winds (e.g., $>45 \text{ m s}^{-1}$) appear to be enhanced within the channel between the Taiwan terrain and the storm. To quantitatively assess the impact of the induced asymmetric flow in steering the

storm motion, the asymmetric components of the wind fields are calculated by subtracting the symmetric component of the wind (relative to the center with the minimum wind speed) from the total wind field. An “advection wind vector” is thus defined as the average asymmetric flow within the inner circle (e.g., 100-km radius from the center²) of the storm. The asymmetric advection wind vectors at different pressure levels (open arrows in Fig. 8b) indicate the primary steering current for the storm in CTRL is below 500 hPa, which is in good agreement with the motion direction of the simulated storm (bold arrow in Fig. 8b). The magnitude of the average asymmetric winds (4.0 m s^{-1} at 700 hPa and 3.2 m s^{-1} at 600 hPa) is also close to the storm translation speed in CTRL (3.3 m s^{-1}). This close agreement suggests that the low-level northerly jet and the associated advection flow are crucial in deflecting the storm motion from westward to southward. The storm motion in CTRL then gradually slows and turns back to the north during the following hours (Figs. 5c–f). The meridional deflection during the simulated cyclonic loop is roughly 60 km before the storm makes landfall in Taiwan (Fig. 4). It will be shown (later in Fig. 14a) that the advection wind vectors match most closely the moving vectors of the simulated vortex when it is making the looping motion.

b. Sensitivity of storm-track deflection to the terrain height

Four sensitivity experiments, denoted H70, H40, H10, and FLAT, are conducted in which the terrain height of Taiwan at each grid is reduced to 70%, 40%, 10%, and 0% of the terrain height in CTRL, respectively, to demonstrate the impact of the Taiwan terrain on the track deflection. In FLAT, the Taiwan terrain is set to 1 m in elevation, while the land–sea attributes remain unchanged.

When the terrain height is reduced in the H70 and H40 simulations, the storm still experiences a looped

path prior to landfall in Taiwan (Figs. 9a,b), except that the magnitude of the track deflection is smaller than that in the CTRL simulation. With further reductions of the terrain height in the H10 and FLAT simulations, a relatively straight-moving storm track toward Taiwan is predicted with a very small deflection (Figs. 9c,d). It will be shown later in this section that the differences in simulated tracks may be attributed to the different intensity of the low-level northerly jet on the western side of storm.

As indicated in the Hovmöller diagrams in Fig. 10a for the CTRL simulation, the area of higher V_{\max} before about 31 h is on the northeastern to north-northeastern quadrant. Between 31 and 35 h, the maximum shifts to the western side of the storm (Fig. 10a), which is attributed above to the channeling effect that then has an impact on the storm motion. When the storm moves closer to the Taiwan coast, the low-level northerly jet decreases quickly since the western quadrant of the eyewall is weakened by surface friction. As a result, the area of higher V_{\max} shifts back to the eastern side of the storm in CTRL after about 38 h (Fig. 10a).

In H70 and H40 (Figs. 10b,c), a low-level northerly jet is also simulated during the period when the higher V_{\max} area shifts from the north-northeastern side to the west of the storm center. The peak 900-hPa wind speeds of the low-level northerly jet in H70 and H40 reach around 55.4 and 54.9 m s^{-1} , respectively, which are slightly weaker than that of the CTRL experiment (about 56.0 m s^{-1} ; Fig. 10a). The presence of peak winds in the west sector of the eyewall suggests that the channeling effect in the H70 and H40 simulations remains strong enough to induce a northerly advection flow, and thus leads to the looping motion of the storm (Figs. 9a,b). After the looping motion, the area of higher V_{\max} in both H70 and H40 also shifts back to the eastern side of the storm as it moves closer to Taiwan.

When the terrain height is drastically reduced in H10, the channeling northerly winds become much weaker (Fig. 10d). Hence, the storm H10 exhibits a relatively straight track with only a slightly southward deflection before landfall (Fig. 9c). A similar result is found in the sensitivity experiment with a flat terrain (FLAT; see Figs. 10e and 9d). When the Taiwan terrain is removed (experiment NT), the area of higher V_{\max} is generally located on the northeastern and eastern sides of the simulated storm throughout the 24–43-h period. In summary, the reduction of the height of the Taiwan terrain weakens the low-level northerly jet in a manner consistent with the reduced magnitude of the track deflection.

At 33 h, the simulated storms in both H70 and H40

² It is well known that the TC basically moves following the large-scale steering flow, generally defined as the environmental current horizontally and vertically averaged over the area surrounding the storm center (therefore removing the symmetric component of the strong cyclonic flow) (Chan and Gray 1982). Other studies (e.g., Wu and Emanuel 1995a,b) suggested that with very high-quality data (such as the radar data in Roux and Marks 1991), the averaged flow within the inner-core region can be used to represent the steering flow. In this study, because the asymmetric winds associated with the terrain-induced low-level northerly jet are primarily confined within the inner-core region of the storm, the asymmetric flow within a TC inner core (a radius of 100 km) should be representative in steering the storm as it moves close to the east coast of Taiwan.

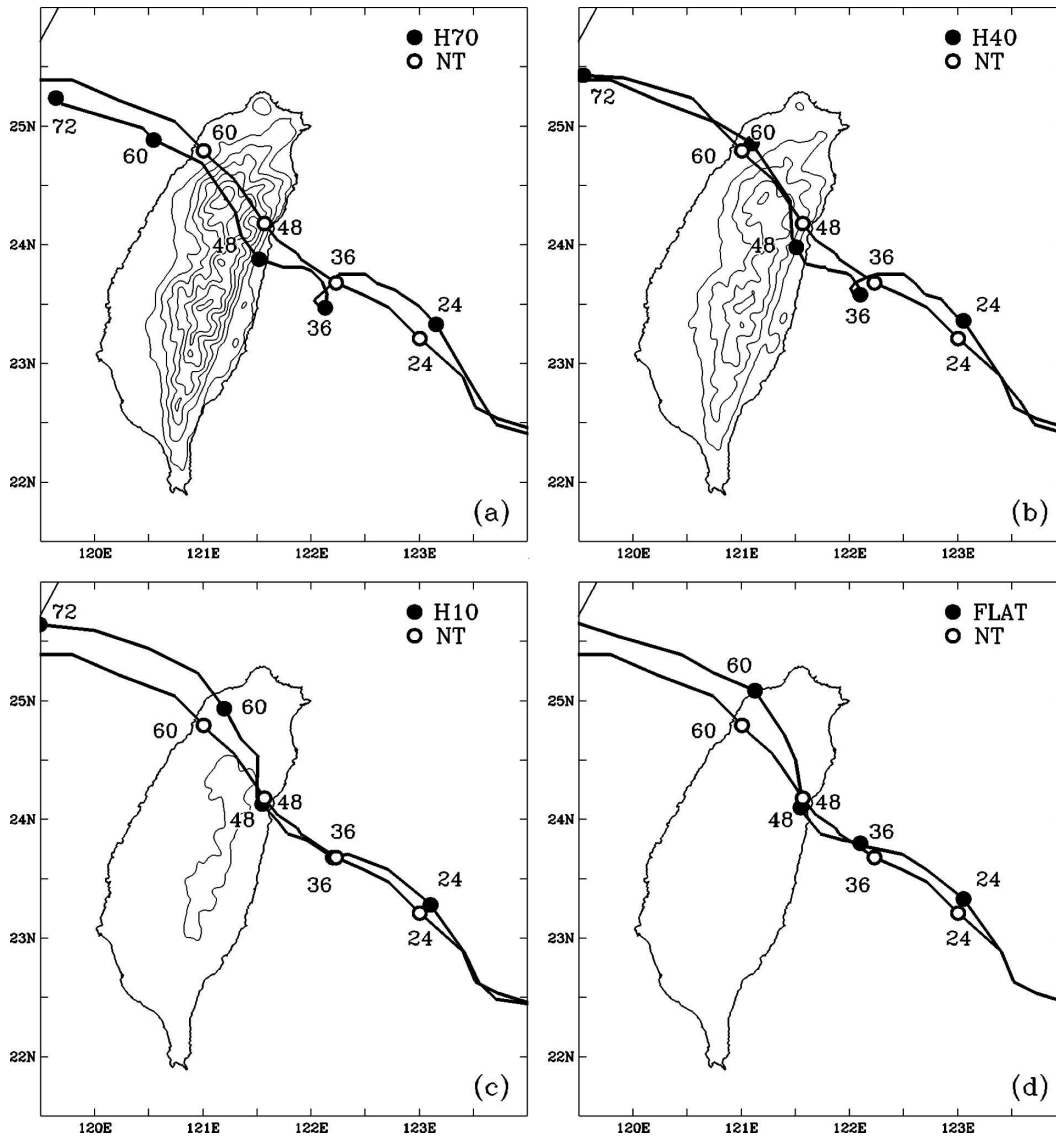


FIG. 9. Comparison of the simulated tracks in the NT experiment (open circles) and the (a) H70, (b) H40, (c) H10, and (d) FLAT experiments (solid circles). The terrain heights (thin lines) in these sensitivity studies start from 200 m high and have a contour interval of 300 m.

are moving southwestward with the strongest winds in the western semicircles. The advection wind vectors below 600 hPa (see open arrows in Figs. 11a,b) are also pointing to the southwest, which agrees reasonably well with the storm movement in H70 and H40 (boldface arrows in Figs. 11a,b). However, the region of stronger winds in the H10 and FLAT simulations generally appears in the north-northeastern and northern quadrants (Figs. 10d,e). The model storms in H10 and FLAT are moving westward with translation speed of 1.5 and 2.3 m s^{-1} , respectively, which agree well with the advection wind vectors estimated from the asymmetric winds of about 1.6 and 2.0 m s^{-1} at 700 hPa (Figs. 11c,d).

The above sensitivity tests demonstrate that the storm motion near Taiwan is sensitive to the terrain height because the reduced terrain height experiments generate a weaker low-level northerly jet and therefore smaller magnitude of the southward deflections.

c. Impact of the initial vortex structure

Changing the structure parameter (α) of the Rankine vortex changes the horizontal scale of the tangential wind component of the initial vortex. In this section, four sensitivity experiments, denoted A35, A47, A35_NT, and A47_NT, which correspond to α values of 0.35 and 0.47 (see Table 1), are performed to study the

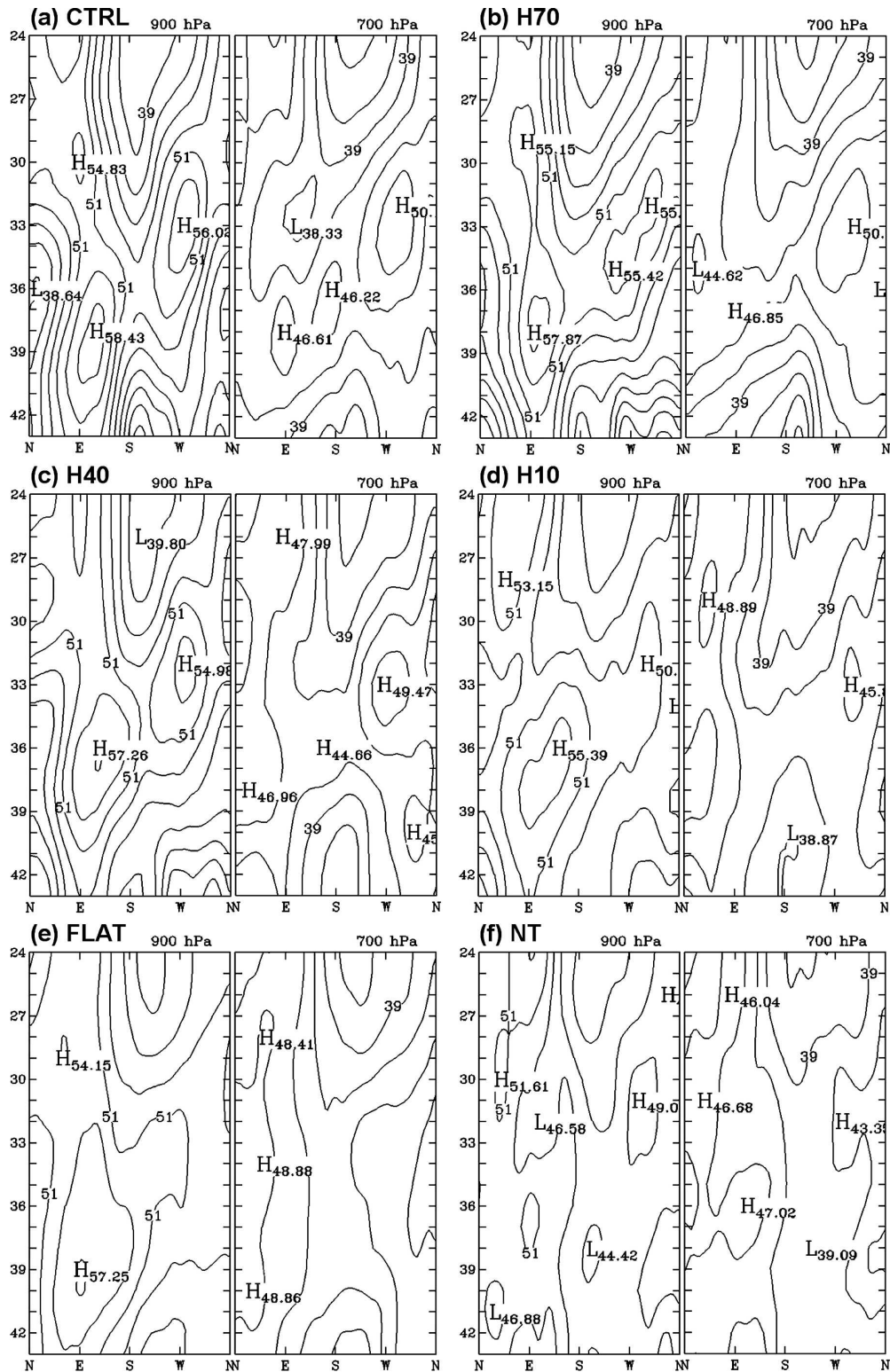


FIG. 10. Time-azimuth Hovmöller diagram of simulated maximum tangential wind speed inside the 100-km radius (with contour interval of 3 m s^{-1}) at (left) 900 and (right) 700 hPa from 24 to 43 h of experiments (a) CTRL, (b) H70, (c) H40, (d) H10, (e) FLAT, and (f) NT.

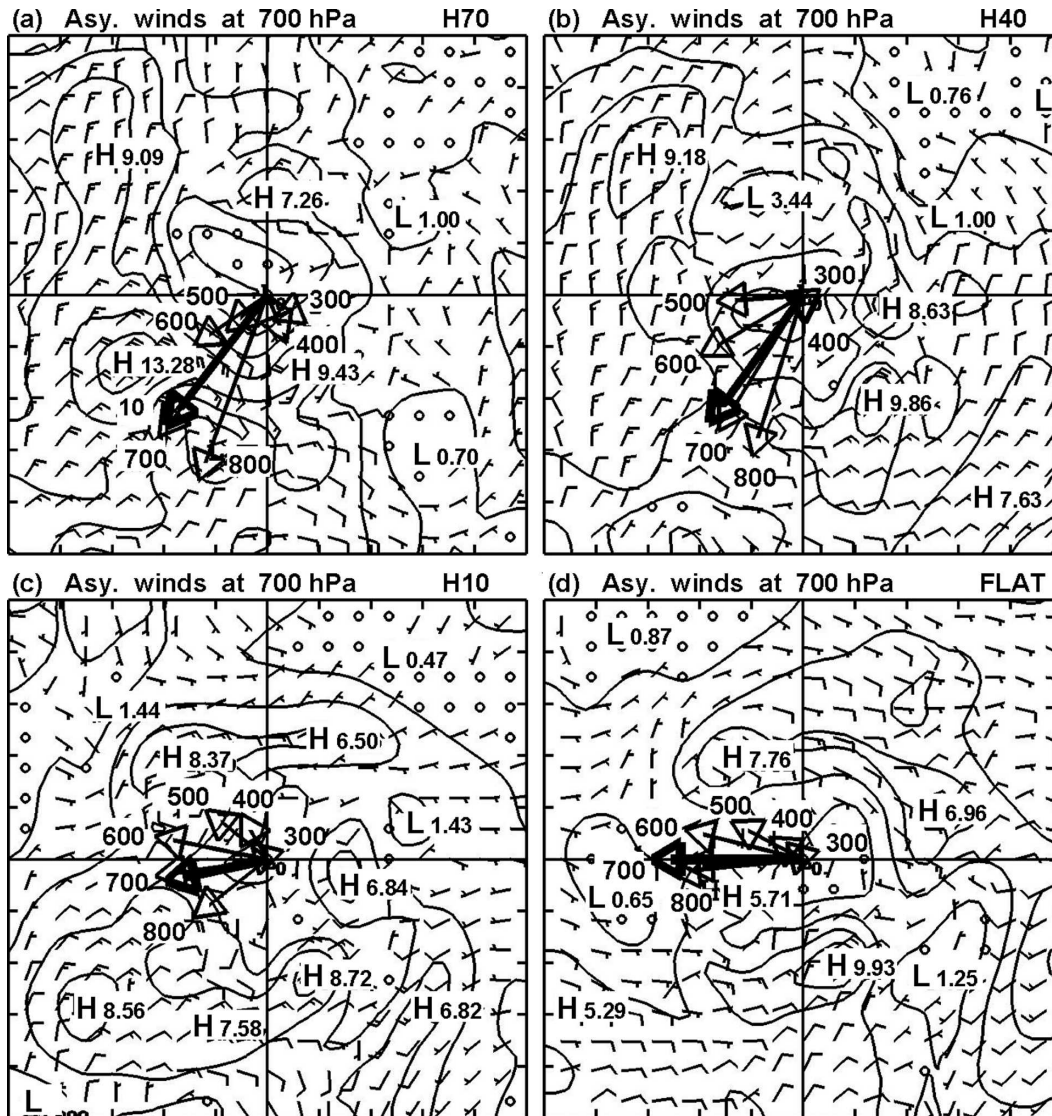


FIG. 11. Simulated asymmetric wind fields (contour interval of 2 m s^{-1}) at 700 hPa after 33-h model simulation for experiments (a) H70, (b) H40, (c) H10, and (d) FLAT (one full wind barb = 5 m s^{-1}). The boldface arrows indicate the storm motion vector (H70: 2.5 m s^{-1} , H40: 2.4 m s^{-1} , H10: 1.5 m s^{-1} , and FLAT: 2.3 m s^{-1}). The open arrows in each panel show the average asymmetric flow within 100-km radius from the storm center at the indicated vertical levels (hPa). The domain in each panel is $200 \text{ km} \times 200 \text{ km}$.

impact of the different vortex structures on the track deflection as the storm vortex approaches Taiwan. The experiment setup in A35_NT and A47_NT is the same as in A35 and A47, except that the Taiwan terrain is removed.

The azimuthal mean tangential wind speed at the lowest model level of the vortex (after a 12-h model integration) for the three experiments are compared in Fig. 12. Experiments A35 and A47 have stronger and larger vortices with maximum mean tangential winds at the lowest model level of about 52.3 and 47.4 m s^{-1} compared with the maximum mean tangential wind

speed of about 42.1 m s^{-1} in CTRL. The corresponding minimum MSLPs for the A35, A47, and CTRL are 941, 952, and 960 hPa, respectively. The RMWs of the storms in A35 (about 70 km) and A47 (about 65 km) are also slightly larger than that of the storm in CTRL (about 60 km).

Past studies (e.g., Elsberry 1995) have shown that storms of different intensities are steered by different atmospheric steering flows (e.g., shallower for weaker and deeper for stronger storms), and the beta drift depends on the storm size. In comparing Fig. 13 with Fig. 4, it is seen that these larger storms move faster and

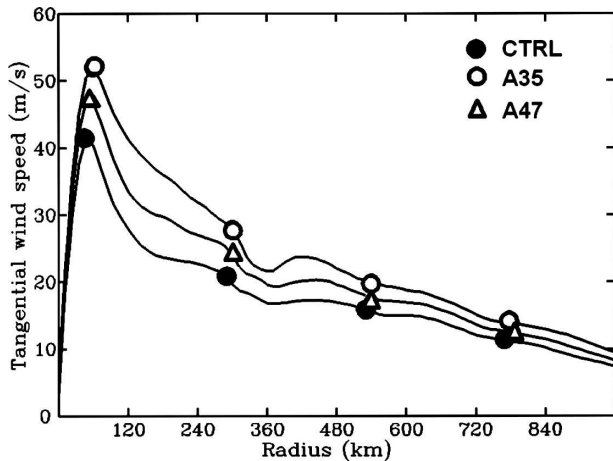


FIG. 12. Radial distribution of azimuthal mean tangential wind speeds (m s^{-1}) for A35 (open circles), A47 (triangles), and CTRL (solid circles) experiments after 12-h model simulation.

have earlier landfall times. Although the A35 and A47 storms are deflected southward compared with the tracks in A35_NT and A47_NT, the simulated tracks are toward the west-northwest without making a loop during the prelandfall period.

The relatively straight tracks in the A35 and A47 experiments are primarily associated with two factors. First, the larger and stronger storms in the A35 and A47 are less susceptible to the topographic deflection than the storm in CTRL as suggested by previous studies (e.g., Yeh and Elsberry 1993a,b; Lin et al. 2005). A faster-moving vortex has less time to interact with the

terrain and experiences smaller track deflection as it approaches Taiwan (e.g., Chang 1982; Bender et al. 1987). In this study, for a given magnitude of southward advection flow (e.g., 3.0 m s^{-1}), the faster-moving A35 storm (about 4.9 m s^{-1} during 12–24-h integration) would experience less southward turn as compared with the slower-moving storm in CTRL (about 3.5 m s^{-1} during 12–24-h integration) and thus has a relatively straight track toward Taiwan without making a loop. Second, the average southward steering flow associated with the A35 and A47 storms is smaller than that of CTRL. Recall the looping motion of the storm in CTRL is initiated through a sharp southward turn (Fig. 4) when the region of strongest winds shifts from the eastern side to the western side of the eyewall (see Fig. 6). In CTRL, the low-level northerly jet in the western quadrant is the strongest wind and these asymmetric winds lead to a northerly asymmetric advection flow that effectively steers the storm southward (Fig. 14a). Similar to the CTRL, the maximum horizontal winds of greater than 50 m s^{-1} are simulated between the Taiwan terrain and the storm in A35 and A47 as well (not shown), which deflects the simulated storm southward compared with the simulations without the Taiwan terrain (see Fig. 13). However, the strongest winds (in the range of $60\text{--}65 \text{ m s}^{-1}$) are in the eastern quadrant of the storms in both the A35 and A47 simulations so that the southward components of the advection flow in A35 are much less than in the CTRL (Fig. 14b; similar for A47, not shown).

In summary, the first factor implies that the faster-

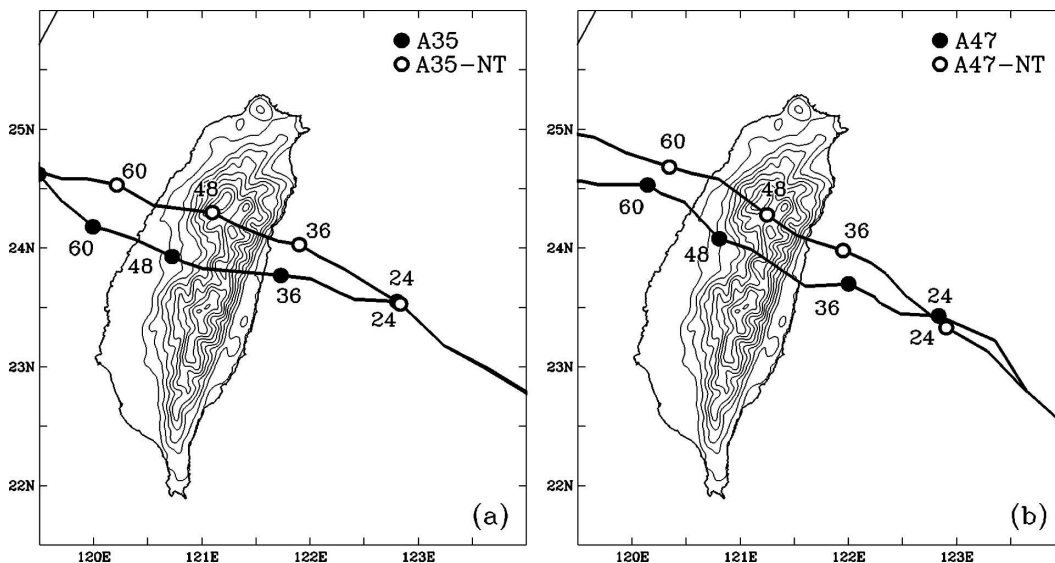


FIG. 13. Simulated tracks of (a) A35 (solid circles) and A35_NT (open circles) and (b) A47 (solid circles) and A47_NT (open circles). Taiwan's terrain heights (thin lines) in experiments A35 and A47 start from 200 m high and have a contour interval of 300 m.

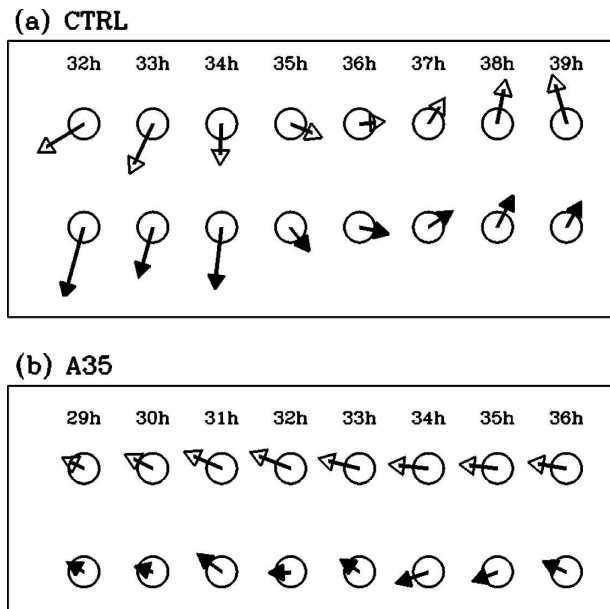


FIG. 14. Time series of (top row) simulated storm motion (open arrows) and (bottom row) the area-mean asymmetric flow within 100-km radius from the storm center at 700 hPa (solid arrows) for experiments (a) CTRL and (b) A35. The circle shows the scale of 1.5 m s^{-1} .

moving storm has less time to deflect southward, which is the key mechanism to prevent the looping path. The second factor contributes to a smaller southward deflection since the southward steering flow is weaker.

It should be noted that the proper value of parameter α for a typhoon can be estimated by the observations from an unmanned aerial vehicle. Lin (2006) notes the first-ever eyewall penetration by Aerosonde was made in Supertyphoon Longwang (2005) on 1 October. Lin (2006) found that the optimal value of α for Longwang is about 0.4 by analyzing the tangential wind profile associated with the flight mission. An interesting feature is that Longwang followed a straight track without making a loop prior to its landfall on the shoreline near Hua-Lien, Taiwan. The track of Longwang is consistent with the simulation results in A35 and A47.

5. Discussion and conclusions

This series of numerical simulations examines the physical processes responsible for the significant track deflection and peculiar looping motion of Supertyphoon Haitang (2005) prior to its landfall in Taiwan. All experiments are performed with the highest horizontal resolution of 4 km using the WRF-ARW modeling system, version 2.0.3. All the 72-h model simulations begin at 0000 UTC 17 July 2005.

In the control experiment with full Taiwan terrain, the simulated track agrees well with Haitang's best track during the 72-h integration, especially during the looping motion off the east coast of Taiwan and the landfall location north of Hua-Lien, Taiwan. In the simulation without the Taiwan terrain, the looping motion disappears, which suggests that the presence of the Taiwan terrain plays a significant role in the track deflection. When Haitang was about 60 km east of Taiwan, the low-level flow on the western side of storm center accelerated because the air parcels originate from a relatively wider area. This channeling effect as the inner-core circulation of the approaching typhoon is constrained because of the presence of the Taiwan terrain (e.g., Lin et al. 2005). Through the channeling effect, a low-level northerly jet forms in the western quadrant of the storm that eventually becomes the strongest winds of the CTRL storm. The asymmetric winds induce a southward advection flow that causes the storm to turn sharply southward. During this stage, the movement of the simulated storm agrees well with the advection wind vectors at the 700- and 600-hPa pressure levels. Moreover, the time series of the advection flow illustrates that the advection wind vectors rotate cyclonically with time in a similar manner as the motion vectors of the simulated vortex. These simulations demonstrate that the advection flow caused by the inner-core asymmetric winds is important in causing the looping motion of Haitang prior to the landfall.

Sensitivity experiments in which the Taiwan terrain is artificially modified indicate that as the terrain height decreases, the magnitude of the storm-track deflection is reduced. For experiments with the terrain height decreased to 70% or 40% of that in CTRL, the simulated storm still exhibits a looping path before landfall as long as the low-level northerly jet has the strongest winds in the storm and the advection wind vectors rotate cyclonically in time. When the terrain height is further reduced to 10% or less of that in CTRL, the looping motion of Haitang disappears since the channeling of winds in the western side of the storm is not strong enough to establish the southward advection flow. In these latter experiments, the strongest winds in the storm are generally in the north-northeastern and northern quadrants. The wind asymmetries tend to correspond to an easterly advection flow that tends to steer the simulated storm westward. These simulations confirm that the high terrain in Taiwan plays a critical role in inducing the strong low-level northerly jet to the west of the center of Haitang, and thus a southward advection flow that leads to the southward drift.

Further experiments are conducted to assess the impact of storms with different intensities and sizes on the

Taiwan-terrain effect. A stronger and larger storm is simulated by using a smaller value of structure parameter (α) in the initial Rankine vortex. The storm in A35 ($\alpha = 0.35$) tends to move faster and has an earlier land-fall time than that of CTRL ($\alpha = 0.6$). Because the strength of the low-level northerly jet (approximately $55\text{--}56\text{ m s}^{-1}$) in A35 is similar to that of CTRL, a strong channeling effect occurs in both simulations as the storm approaches Taiwan. The track differences between the storms of A35 and CTRL are primarily due to two main causes. First, the storm in A35 is a larger, more intense, and more rapidly moving vortex and therefore would be more likely to move across the Taiwan terrain with less track deflection (e.g., Chang 1982; Bender et al. 1987). This factor implies that the faster-moving storm has less time to deflect southward, which is the key mechanism to prevent the looping motion. Second, although a low-level northerly jet is also predicted in the western portion of the A35 storm, the strongest winds associated with the storm are on the eastern side of the storm. In contrast to the CTRL simulation, the wind distribution in the A35 storm has smaller average southward steering (advection), which leads to a smaller southward deflection. These simulations suggest that the two above factors are important for determining the sharp track deflection associated with a typhoon (e.g., Supertyphoon Haitang) moving westward toward the east coast of Taiwan.

Acknowledgments. The authors thank two anonymous reviewers for their insightful and constructive comments, which have helped to improve the content and presentation of the manuscript. We also thank Y.-L. Lin of the North Carolina State University and C.-S. Lee of the National Taiwan University for their useful suggestions on this work, as well as the WRF Help Desk at NCAR. Some assistance from S.-Y. Liou with the graphics is also appreciated. This work is supported by the National Science Council of Taiwan Grants NSC 95-2625-Z-052-004 and NSC 95-2119-M-002-003-AP1.

REFERENCES

- Bender, M. A., R. E. Tuleya, and Y. Kurihara, 1987: A numerical study of the effect of island terrain on tropical cyclones. *Mon. Wea. Rev.*, **115**, 130–155.
- Brand, S., and J. W. Blueloch, 1974: Changes in the characteristics of typhoons crossing the island of Taiwan. *Mon. Wea. Rev.*, **102**, 708–713.
- Chan, J. C. L., and W. M. Gray, 1982: Tropical cyclone movement and surrounding flow relationship. *Mon. Wea. Rev.*, **110**, 1354–1376.
- , and R. T. Williams, 1987: Analytical and numerical studies of the beta-effect in tropical cyclone motion. Part I: Zero mean flow. *J. Atmos. Sci.*, **44**, 1257–1265.
- Chang, C.-P., T.-C. Yeh, and J. M. Chen, 1993: Effects of terrain on the surface structure of typhoons over Taiwan. *Mon. Wea. Rev.*, **121**, 734–752.
- Chang, S. W., 1982: The orographic effects induced by an island mountain range on propagating tropical cyclones. *Mon. Wea. Rev.*, **110**, 1255–1270.
- Chen, S.-H., and J. Dudhia, 2000: Annual report: WRF physics. Air Force Weather Agency, 38 pp. [Available online at <http://www.mmm.ucar.edu/wrf/users/docs/wrf-doc-physics.pdf>.]
- Davis, C. A., and S. Low-Nam, 2001: The NCAR-AFWA tropical cyclone bogussing scheme. NCAR Tech. Note, 13 pp. [Available online at <http://www.mmm.ucar.edu/mm5/mm5v3/tc-report.pdf>.]
- Dudhia, J., 1989: Numerical study of convection observed during the winter monsoon experiment using a mesoscale two-dimensional model. *J. Atmos. Sci.*, **46**, 3077–3107.
- Elsberry, R. L., 1995: Tropical cyclone motion. *Global Perspectives on Tropical Cyclones*, R. L. Elsberry, Ed., World Meteorological Organization, 106–197.
- , and F. D. Marks, 1999: The Hurricane Landfall Workshop summary. *Bull. Amer. Meteor. Soc.*, **80**, 683–685.
- Fiorino, M. J., and R. L. Elsberry, 1989: Some aspects of vortex structure related to tropical cyclone motion. *J. Atmos. Sci.*, **46**, 975–990.
- Hong, S.-Y., J. Dudhia, and Y. Noh, 2003: A new vertical diffusion package with explicit treatment of the entrainment processes. *Proc. Int. Workshop on NWP Models for Heavy Precipitation in Asia and Pacific Areas*, Tokyo, Japan, Japan Meteorological Agency, 52–58.
- , —, and S.-H. Chen, 2004: A revised approach to ice microphysical processes for the bulk parameterization of clouds and precipitation. *Mon. Wea. Rev.*, **132**, 103–120.
- Jian, G.-J., C.-S. Lee, and G. T. J. Chen, 2006: Numerical simulation of Typhoon Dot (1990) during TCM-90: Typhoon Dot's discontinuous track across Taiwan. *Terr. Atmos. Oceanic Sci.*, **17**, 23–52.
- Kain, J. S., 2004: The Kain–Fritsch convective parameterization: An update. *J. Appl. Meteor.*, **43**, 170–181.
- Lin, P.-H., 2006: The first successful typhoon eyewall-penetration reconnaissance flight mission conducted by the unmanned aerial vehicle, Aerosonde. *Bull. Amer. Meteor. Soc.*, **87**, 1481–1483.
- Lin, Y.-L., J. Han, D. W. Hamilton, and C.-Y. Huang, 1999: Orographic influence on a drifting cyclone. *J. Atmos. Sci.*, **56**, 534–562.
- , S.-Y. Chen, C. M. Hill, and C.-Y. Huang, 2005: Control parameters for the influence of a mesoscale mountain range on cyclone track continuity and deflection. *J. Atmos. Sci.*, **62**, 1849–1866.
- Marks, F. D., and L. K. Shay, 1998: Landfalling tropical cyclones: Forecasting problems and associated research opportunities. *Bull. Amer. Meteor. Soc.*, **79**, 305–323.
- Miller, B. I., 1967: Characteristics of hurricanes. *Science*, **157**, 1389–1399.
- Mlawer, E. J., S. J. Taubman, P. D. Brown, M. J. Iacono, and S. A. Clough, 1997: Radiative transfer for inhomogeneous atmospheres: RRTM, a validated correlated- k model for the longwave. *J. Geophys. Res.*, **102**, 16 663–16 682.
- Neumann, C. J., 1979: On the use of deep-layer mean geopotential height fields in statistical prediction of tropical cyclone motion. Preprints, *Sixth Conf. on Probability and Statistics in Atmosphere Sciences*, Banff, AB, Canada, Amer. Meteor. Soc., 32–38.

- Peng, M. S., and S. W. Chang, 2002: Numerical forecasting experiments on Typhoon Herb (1996). *J. Meteor. Soc. Japan*, **80**, 1325–1338.
- Roux, F., and F. D. Marks Jr., 1991: Eyewall evolution in Hurricane Hugo deduced from successive airborne Doppler observations. Preprints, *19th Conf. on Hurricanes and Tropical Meteorology*, Miami, FL, Amer. Meteor. Soc., 558–563.
- Skamarock, W. C., J. B. Klemp, J. Dudhia, D. O. Gill, D. M. Barker, W. Wang, and J. G. Powers, 2005: A description of the Advanced Research WRF Version 2. NCAR Tech. Note NCAR/TN-468+STR, 88 pp.
- Wang, S.-T., 1980: Prediction of the movement and strength of typhoons in Taiwan and its vicinity (in Chinese). National Science Council Research Rep. 108, Taipei, Taiwan, 100 pp.
- Willoughby, H. E., 1990: Temporal changes of the primary circulation in tropical cyclones. *J. Atmos. Sci.*, **47**, 242–264.
- , 1992: Linear motion of a shallow water barotropic vortex as an initial-value problem. *J. Atmos. Sci.*, **49**, 2015–2031.
- Wu, C.-C., 2001: Numerical simulation of Typhoon Gladys (1994) and its interaction with Taiwan terrain using the GFDL hurricane model. *Mon. Wea. Rev.*, **129**, 1533–1549.
- , and K. A. Emanuel, 1993: Interaction of a baroclinic vortex with background shear: Application to hurricane movement. *J. Atmos. Sci.*, **50**, 62–76.
- , and —, 1995a: Potential vorticity diagnostics of hurricane movement. Part I: A case study of Hurricane Bob (1991). *Mon. Wea. Rev.*, **123**, 69–92.
- , and —, 1995b: Potential vorticity diagnostics of hurricane movement. Part II: Tropical Storm Ana (1991) and Hurricane Andrew (1992). *Mon. Wea. Rev.*, **123**, 93–109.
- , and Y.-H. Kuo, 1999: Typhoons affecting Taiwan: Current understanding and future challenges. *Bull. Amer. Meteor. Soc.*, **80**, 67–80.
- , T.-H. Yen, Y.-H. Kuo, and W. Wang, 2002: Rainfall simulation associated with Typhoon Herb (1996) near Taiwan. Part I: The topographic effect. *Wea. Forecasting*, **17**, 1001–1015.
- Wu, L., and B. Wang, 2001a: Effects of convective heating on movement and vertical coupling of tropical cyclones: A numerical study. *J. Atmos. Sci.*, **58**, 3639–3649.
- , and —, 2001b: Movement and vertical coupling of diabatic baroclinic tropical cyclones. *J. Atmos. Sci.*, **58**, 1801–1814.
- Yeh, T.-C., and R. L. Elsberry, 1993a: Interaction of typhoons with the Taiwan orography. Part I: Upstream track deflections. *Mon. Wea. Rev.*, **121**, 3193–3212.
- , and —, 1993b: Interaction of typhoons with the Taiwan orography. Part II: Continuous and discontinuous tracks across the island. *Mon. Wea. Rev.*, **121**, 3213–3233.